ACS APPLIED MATERIALS & INTERFACES

Research Article

www.acsami.org

Eu^{3+}-Doped $NaGdF_4$ Nanocrystal Down-Converting Layer for Efficient Dye-Sensitized Solar Cells

Jie Shen,[†] Zhiqiang Li,[‡] Rui Cheng,[†] Qi Luo,[†] Yudan Luo,[†] Yiwei Chen,[†] Xiaohong Chen,[†] Zhuo Sun,[†] and Sumei Huang*[,†]

[†]Engineering Research Center for Nanophotonics & Advanced Instrument, Ministry of Education, Department of Physics, East China Normal University, North Zhongshan Rd. 3663, Shanghai 200062, People's Republic of China

[‡]Faculty of Engineering, Univeristy of Nottingham, Nottingham, NG7 2RD, United Kingdom

ABSTRACT: We present for the first time the synthesis of Eu^{3+}-doped β-phase sodium gadolinium fluoride ($NaGdF_4$:Eu) nanocrystals (NCs) using a hydrothermal method and the application of down conversion (DC) $NaGdF_4$:Eu NCs to efficient dye-sensitized solar cells (DSSCs). The as-prepared $NaGdF_4:Eu^{3+}$ NCs were characterized by X-ray diffraction, photoluminescence spectrometry, and scanning and transmission electron microscopy. DC layers consisting of poly(methyl methacrylate) (PMMA) doped with luminescent $NaGdF_4:Eu^{3+}$ were prepared and attached onto the back of a prefabricated TiO_2 anode to form a more efficient DSSC, compared with a device based on a pure TiO_2 electrode. The influences of both doped and undoped $NaGdF_4$ NC layers on the photovoltaic devices were compared and evaluated by the measurement of the device's incident-photon-to-current efficiency (IPCE). An obvious increase in IPCE was observed when the DC layer was added in the device. As the down-converted photons can be reabsorbed within DSSCs to generate photocurrent, the DSSC with a 100 nm thick $NaGdF_4:Eu^{3+}$ DC-PMMA layer improved photoelectric conversion efficiency by 4.5% relative to the uncoated solar cell. The experiments conclude that $NaGdF_4:Eu^{3+}$ nanocrystals mainly act as luminescent DC centers and light scatterers in the ultraviolet and visible domains, respectively, for enhancing the spectral response of the device in the measured spectral regime.

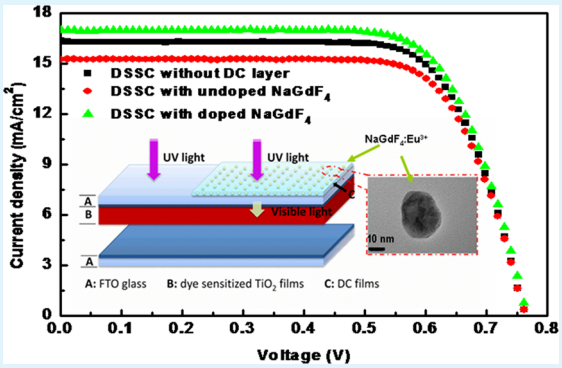

KEYWORDS: *down-converting material, lanthanide-doped, $NaGdF_4$, dye-sensitized solar cell, nanocrystal*

1. INTRODUCTION

The dye-sensitized solar cell (DSSC) was first developed by O'Regan and Grätzel in 1991.[1] The photoelectric conversion efficiency was about 7.1−7.9% under simulated solar light irradiation at that time. Since then, a tremendous amount of research has been conducted to increase the efficiency of the solar cell. The conversion efficiency went up to 11.1% in 2006,[2] and more recently, the efficiency was up to 13% where the dye was a porphyrin dye (coded SM315) with a donor−π-bridge−acceptor structure, and the redox couple was composed of Co^{2+}/Co^{3+} instead of I^-/I_3^-.[3] However, the cells still suffered from relatively low performance and poor stability compared with dominant silicon solar cells. Many research groups and organizations have made new efforts to further promote research and improvement of the efficiency and stability of DSSCs.

In DSSCs, mesoscopic structured TiO_2 films on fluorine-doped tin oxide (FTO)-coated glass slides are typically used as photoanodes, and the TiO_2 films provide large surface areas for anchoring the light-capturing dye molecules. When the sunlight is irradiated onto the device, the dye molecules are excited by absorption of photons. The excited sensitizer molecules rapidly inject electrons into the conduction band of the TiO_2, from which the injected electrons move to the conducting layer on the top of the glass substrate, and the oxidized dyes are subsequently regenerated by electrons donated from the redox electrolyte.[4−7] Ru-complex sensitizers such as N3 and N719 have been well-known and have demonstrated outstanding power conversion efficiencies. However, the main absorption of dyes N3 and N719 occurs in the 290−700 nm wavelength region.[8−10] This spectral response range is very narrow compared to the wavelength range of sunlight. The band of visible light, between 400 and 700 nm, only accounts for 43% of the sun's total radiant energy. Thus, the narrow optical response range of dye molecules limits the efficiency of DSSCs. Moreover, light in the deep ultraviolet (UV) range (wavelengths less than 300 nm) that is incident upon glass-based DSSCs does not participate in photon-to-electron conversion because typical FTO slides usually used borosilicate glass and absorbed a large portion of the UV spectrum. Greater overall incident-photon-to-current efficiency (IPCE) would occur if photons in the deep UV range could be down converted. Therefore, broadening the optical response range of

Received: March 21, 2014
Accepted: September 17, 2014
Published: October 1, 2014

DSSCs from visible light to high-energy UV represents an important method to boost the DSSC conversion efficiency.

Down conversion (DC) is primarily investigated for materials doped with rare-earth (RE) ions. DC happens either on a single ion or through energy transfer processes among various RE ions.[11−18] Different sets of lanthanide ions, for example, Gd^{3+}/Eu^{3+}, RE^{3+}/Yb^{3+} (RE = Tb, Pr, Er, or Tm), and $Gd^{3+}/Tb^{3+}/Er^{3+}$ have exhibited cooperative DC in different hosts, such as crystalline phosphors and noncrystalline glasses.[11−15] Crystalline down-converting phosphors, however, normally consist of grains in submicrometer and micrometer sizes. These phosphors are too large to make the transparent layers required for thin film solar cell applications. In recent years, strong focused attention has been given by many researchers to the development of lanthanide-doped nanocrystals (NCs) due to their many unique properties and potential applications in a variety of optoelectronic devices. Among different hosts for lanthanide-doped NCs, fluoride offers some outstanding advantages over the traditionally used oxide material because the former displays very low energy phonons and can accommodate a high concentration of lanthanide dopant ions, which are essential for facilitating luminescent processes. In particular, DC emission has been demonstrated for certain lanthanide-ion-doped $NaGdF_4$ NCs under deep UV excitation with a quantum efficiency up to 200%.[11,19] $NaGdF_4$ is well-known to be an extremely efficient host lattice for such luminescent processes because Gd^{3+} can serve as an intermediate to permit energy to migrate over the Gd^{3+} sublattice and the migrating energy is sufficiently trapped by the activator ions embedded in host lattice, consequently promoting efficient energy transfer (ET) processes.[20] So far, numerous approaches including coprecipitation, hydrothermal, solid state reaction, and reversed micelle methods have been developed to prepare lanthanide-doped $NaGdF_4$ NCs. These methods are well-described and summarized in the literature.[15,21] However, most of the doping for $NaGdF_4$ has been explored just for synthesizing luminescent nanomaterials.

The concept of integrating a DC layer into a solar cell has attracted significant attention because it removes the load of spectral matching from the semiconductor itself, minimizes the thermalization losses in cells, and moves this task to a separation component.[16−18] Trupke et al. theoretically proved the possibility of increasing solar cell conversion efficiency by applying DC from RE dopants.[16] The calculated maximum efficiency promotion for a crystalline silicon solar cell was 38.6% attaching the spectral converter on the front electrode of the cell. However, the initial work conducted on DSSCs by the introduction of DC layers onto the device might seem unlikely to obtain an improvement for these kinds of devices. Liu et al. synthesized Dy^{3+}-doped $LaVO_4$ NCs and applied the DC luminescent nanomaterials in a film prior to the DSSC.[22] It was found that a DSSC with the DC layer exhibited an 8% lower efficiency than a bare solar cell without using a DC converter, but the lifetime of the former was considerably improved, and its photoelectric conversion efficiency was 23% higher than a device covered with an undoped $LaVO_4$ film. The work demonstrated that DC films of some forms could be employed as a substitute for the UV blocking layer that is needed for long-term stable DSSCs. Moreover, doping titania electrodes with certain lanthanide ions can alter the band edges or surface states of titanium dioxide or improve UV light-capturing of the electrodes through DC luminescence processes,[23−27] providing another method to adjust and improve photoelectric conversion performance of DSSCs. Several papers reported that doped TiO_2 photoanodes are likely to create some positive improvements in the efficiency of photovoltaic (PV) cells.[23,24] For example, the DSSC based on Nb-doped TiO_2 anode achieved an 18.2% higher efficiency than the device based on undoped TiO_2 electrode as reported in our previous work.[23] Eu^{3+}- and Sm^{3+}-doped TiO_2 photoelectrodes also exhibited improved conversion efficiencies compared to that of undoped TiO_2.[24] Despite these highly optimistic achievements, the introduction of a DC film in a preformed photovoltaic device also causes extra interactions with light, leading to additional loss mechanisms, and hence decreasing the efficiency of the device.[16,22,28] To the best of our knowledge, very few reports have demonstrated real enhancement of DSSC photoelectrical efficiency, and especially the device's IPCE, using a DC converter with a RE element addition without interfering with the active films of the photovoltaic cell.

In this work, we report a hydrothermal method to synthesize uniform Eu^{3+}-doped $NaGdF_4$ NCs and their application for DSSCs. The DC layer consisting of poly(methyl methacrylate) (PMMA) doped with luminescent $NaGdF_4:Eu^{3+}$ was applied to the front surface of the preformed TiO_2 anode and worked as both a DC converter and a UV filter for DSSC. With this architectural designs, the DC process in $NaGdF_4:Eu^{3+}$ NCs modified the sunlight spectrum to better match the optical properties of solar cells, as opposed to changing the solar cell itself, enabling the efficiency increase of the underlying solar cell. The influence of the DC converter film on the solar cell was appraised by measuring the device's IPCE under the conditions with and without the DC layer. It was found that in a DSSC with a $NaGdF_4:Eu^{3+}$ DC layer, the UV radiation absorbed by the DC layer was down converted to visible light, which was reabsorbed by dye molecules in the underlying DSSC, improving the cell efficiency by 4.5% compared with that of the referenced DSSC without a DC layer. We have carried out a detailed experimental study on the role of down-converter Eu^{3+}-doped $NaGdF_4$ and proved that the utilization of $NaGdF_4:Eu^{3+}$ phosphors as a DC film is an effective approach to boost the power conversion efficiency of efficient DSSCs.

2. EXPERIMENTAL SECTION

2.1. Synthesis of Down-Conversion $NaGdF_4$:Eu Nanocrystals. $NaGdF_4$:Eu nanocrystals were prepared by modifying the procedures described in references 29 and 30. A deionized water solution (7.5 mL) containing 1.5 g of NaOH was mixed with ethanol (25 mL) and oleic acid (25 mL) under continuous stirring, and then 10 mL of $RECl_3$ (0.2 M, RE = Eu and Gd, $EuCl_3/GdCl_3$ = 30:70 mol %) solution and 5 mL of NH_4F (2 M) was added. The resultant mixture was transferred into a 100 mL Teflon-lined stainless autoclave. The autoclave was heated at 200 °C for 2 h and subsequently cooled to room temperature. The resultant nanocrystals were collected, washed, and dried in vacuum. Finally, the nanocrystals were dispersed evenly in a PMMA−acetone solution to produce a DC-PMMA mixture with a concentration of 2 mg mL^{-1} of DC luminescent NCs. For a comparison study, undoped $NaGdF_4$ nanocrystals were fabricated without using $EuCl_3$ under the same hydrothermal conditions for $NaGdF_4$:Eu NCs, and an undoped $NaGdF_4$−PMMA mixture with the same concentration of $NaGdF_4$ NCs was prepared.

2.2. Preparation of the DSSCs. DSSCs with thermally deposited Pt were fabricated. The TiO_2 working electrodes were prepared using screen-printing double-layered TiO_2 with a total thickness of about 14 μm on the FTO glass plates following the same procedure that was described in our previous work.[31] The as-prepared photoanodes were dipped in an N719 dye solution (0.5 mM in acetonitrile and *tert*-butyl

alcohol) for 20 h. The dye-covered photoanode and Pt counter electrode were assembled into a sandwich-type cell and sealed with a 25 μm thick Surlyn 1702 (Dupont) gasket. A drop of the electrolyte, a solution of 0.05 M I_2, 1 M MPII, 0.5 M guanidine thiocyanate, and 0.5 M *tert*-buthylpyridine in acetonitrile, was deposited through the hole in the back of the counter electrode. The electrolyte was introduced into the cell via capillary action. Then, the hole was sealed using the same Surlyn film and a cover glass (0.7 mm thick). Finally, $NaGdF_4$:Eu NCs were deposited on the as-prepared DSSC solar cell front glass surface by spin-coating of the formed DC $NaGdF_4$:Eu–PMMA solution and dried in air. The thickness of the DC-PMMA layer on the front glass was controlled by the number of coating cycles. The obtained DSSCs with one and two DC coating cycles were labeled Cell 3 and Cell 4, respectively. Figure 1 shows a schematic diagram of downshift luminescent layer coated DSSC and illustrates the principle of the solar cell. For comparison, the DSSC with a front bare FTO glass was used as a reference device (referred to as ref cell), and cells with front-coated films of pure PMMA or undoped $NaGdF_4$–PMMA after one coating cycle were also fabricated (labeled Cell 1 and Cell 2, respectively).

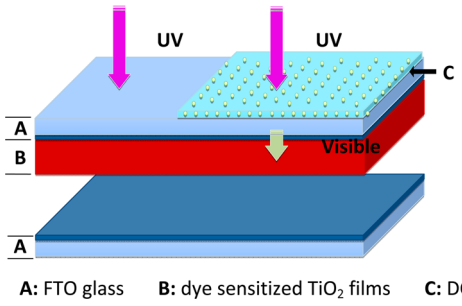

Figure 1. Schematic diagram of downshift luminescent layer coated DSSC.

2.3. Characterization of Samples. The surface morphology and the nanostructure of the grown DC NCs were characterized by field emission scanning electron microscopy (FESEM, Hitachi S4800, Japan). The chemical compositions of these nanophosphors were examined by an energy dispersive X-ray spectrometer attached to Hitachi FESEM. Their optical and crystallographic properties were determined using UV–vis spectrophotometry (Hitachi, U-3900) and X-ray diffraction (XRD) (Rigaku DMAX 2500, Japan), respectively. Transmission electron microscopy (TEM) and selective area electron diffraction (SAED) images were captured with a JEOL 2010 TEM at 200 kV. Fluorescence spectra were collected by a spectrophotometer (HORIBA Jobin Yvon, Fluoromax-4) assisted with a 980 nm near-infrared laser. Photovoltaic measurements were conducted by an AM 1.5 solar simulator outfitted with a 1000 W xenon lamp (Model No. 91192, Oriel Instruments, Stratford, CT). The power of the simulated light was calibrated to be 100 mW cm^{-2} using a standard silicon cell (Newport Corporation, Irvine, CA). Incident photon-to-electron conversion efficiency (IPCE) measurements on DSSCs were performed from 200 to 1000 nm in wavelength with a 200 W Hg (Xe) Lamp (Model 6289) and a flange mount calibrated UV–Si photodiode sensor (Model 71675). The active area of DSSCs is 0.25 cm^2.

3. RESULTS AND DISCUSSION

The $NaGdF_4$:Eu^{3+} NCs deposited in a Teflon-lined autoclave at 200 °C for 2 h were examined by TEM and FESEM. Figure 2a,b shows the typical TEM images of $NaGdF_4$:Eu^{3+} NCs with different magnifications. The high-resolution TEM characterizations (Figure 2b) clearly revealed the crystalline nature of these nanocrystals. The inset of Figure 2b shows their SAED patterns, in which the spotty diffraction rings can be indexed to the specific planes of the hexagonal $NaGdF_4$ lattice. Additionally, the grown $NaGdF_4$:Eu^{3+} NCs exhibited uniform crystallite diameters in the range of 20–30 nm, as shown in Figure 2a. FESEM characterizations (Figure 2c) were conducted to further explain the morphological features of the NCs. The results also indicated that the $NaGdF_4$:Eu^{3+} NCs have good size and shape uniformity. The structural characteristics of the nanocrystals were further examined by XRD. As shown from the XRD pattern in Figure 2d, all of the diffraction peak positions and intensities were in good agreement with the data for the hexagonal-phase $NaGdF_4$ crystals (Standard PDF card: 27-0699). The results are consistent with TEM analysis. The atomic compositions of the $NaGdF_4$:Eu^{3+} NCs were determined by energy-dispersive X-ray analysis (EDX), shown in Figure 2e. The atomic ratio of Na/Gd/F/Eu was found to be 1:0.69:3.89:0.31, which is very close to the value (1:0.7:4:0.30).

Figure 3 shows the room-temperature photoluminescence (PL) excitation and DC emission spectra of Eu^{3+} in the deposited $NaGdF_4$:Eu NCs, which are dispersed as a 2 mg mL^{-1} colloid in ethanol. From Figure 3, under a single light of 274 or 395 nm in the UV region, the NaGdF4:Eu NCs show intensive multicolor visible emissions. As direct neighbors in the lanthanide series, gadolinium and europium have very similar properties. When Eu^{3+} is incorporated as a dopant ion into the $NaGdF_4$ host lattice, the Eu^{3+} ions can be excited not only through their 4f–4f transitions but also through ET from Gd^{3+} to Eu^{3+}.[19,32,33] As a result, the Eu^{3+}-excitation spectrum of $NaGdF_4$ successfully doped with europium has an intense peak at 274 nm which is ascribed to the $^8S_{7/2} \rightarrow {}^6I_J$ transitions of Gd^{3+}. This peak is observed in the excitation spectrum of our $NaGdF_4$ NCs, as shown in the graph on the left side of Figure 3a. The PL excitation spectrum of Eu $^{3+}$ shows a dominant sharp excitation line centered at ~274 nm, while the emission spectrum exhibits the fingerprint of Eu^{3+} ions upon indirect excitation at 274 nm, as shown in the graph on the right side of Figure 3a. This result suggests that the Eu^{3+} emission can be realized by an ET process, in which Gd^{3+} ions absorb the UV excitation light as a sensitizer, and then circulate energy to the Eu^{3+} activator ions embedded in the host lattice, leading to the overall red emission of Eu^{3+}. The DC emission peaks at ~591, 615, and 694 nm can be facilely ascribed to the de-excitation from $^5D_0$ to the $^7F_1$, $^7F_2$, and $^7F_4$ lower-lying levels of Eu^{3+}, respectively,[34] as shown in the graph on the right side of Figure 3a. Figure 3b shows the emission spectrum recorded in the 575–700 nm spectral region under 395 nm excitation, which correspond to $^7F_0 \rightarrow (^5L_J + {}^5G_J)$ absorption transitions of the Eu^{3+} ion. The distinct emission peaks also present at 591, 615, and 694 nm, which derive from $^5D_0$–$^7F_1$, $^5D_0$–$^7F_2$, and $^5D_0$–$^7F_4$ transitions of Eu^{3+}, respectively. In the presented PL spectra under 274 and 395 nm excitation, the positions and relative intensities of the emission lines are the same, as shown in Figure 3a,b. Comparing characteristic emissions of Eu^{3+} ions, the emission located at 615 nm ($^5D_0$–$^7F_2$) is more dominant than that at 591 nm ($^5D_0$–$^7F_1$) in the grown NaGdF4:Eu^{3+} due to the low symmetries of the local crystal fields around Eu^{3+} ions.[33] The measured PL excitation and DC emission spectra are strikingly similar to those provided in earlier reports for Eu^{3+} doped $NaGdF_4$ nanocrystals.[19,35,36]

Figure 4 shows photocurrent density–voltage (J–V) curves of DSSCs with different structured photoanodes under a light intensity of 100 mW cm^{-2}. The resultant photovoltaic parameters are shown in Table 1. As shown in Figure 4 and Table 1, all the assembled cells shared similar fill factor (FF) and open-circuit voltage (V_{oc}) values. The reference DSSC with

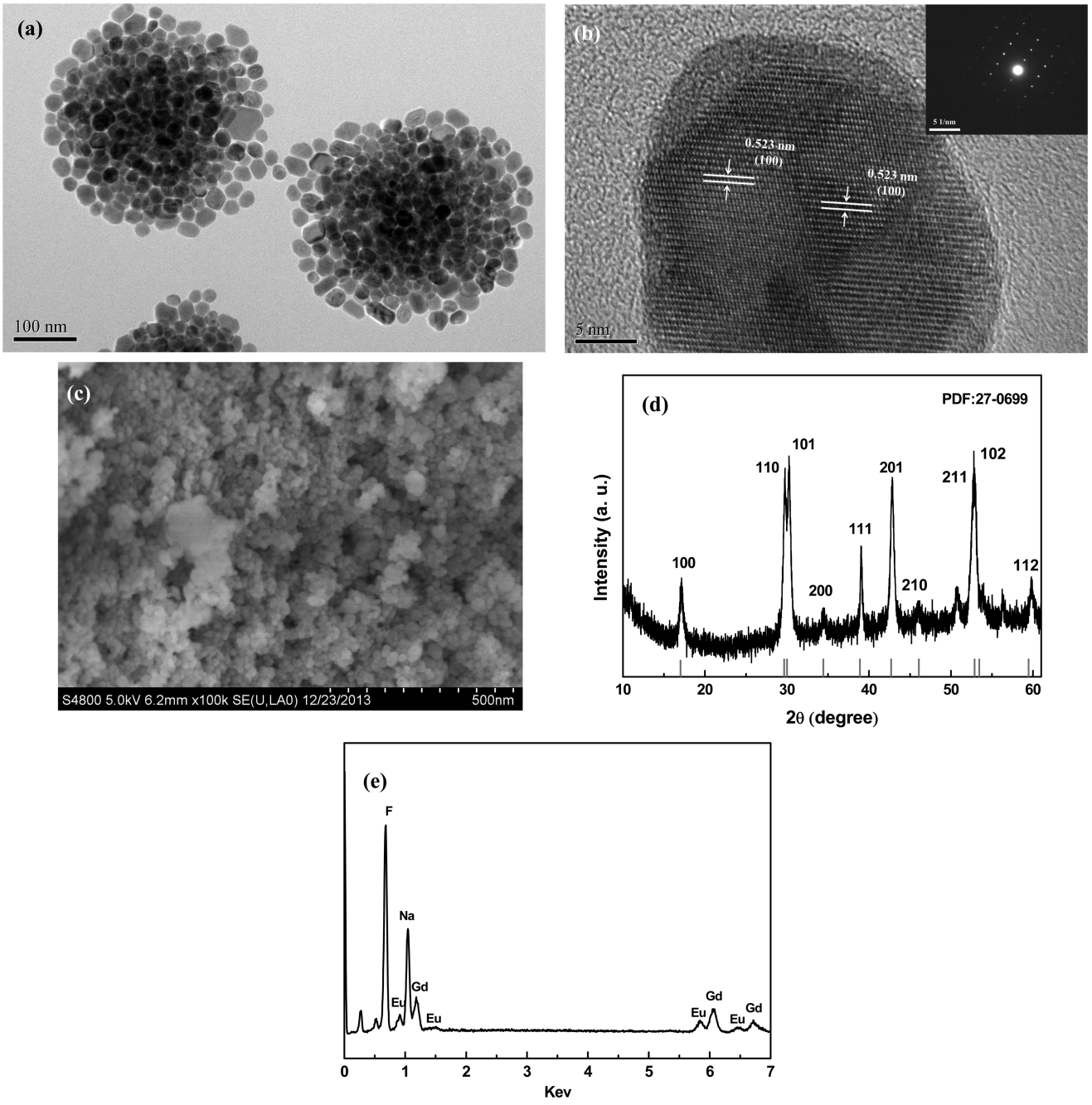

Figure 2. (a and b) TEM images with different magnifications of the $NaGdF_4:Eu^{3+}$ NCs synthesized at 200 °C for 2 h, (b, inset) SAED pattern of $NaGdF_4:Eu^{3+}$ NCs, (c) FESEM images of the $NaGdF_4:Eu^{3+}$ NCs, (d) XRD pattern of the $NaGdF_4:Eu^{3+}$ NCs, and (e) EDX spectrum of the $NaGdF_4:Eu^{3+}$ NCs.

a front bare FTO displays a short-circuit photocurrent density (J_{sc}) of 16.24 mA cm^{-2}, a FF of 72.0%, a V_{oc} of 0.765 V, and a conversion efficiency (η) of 8.94%. The efficiencies of solar cells with front-coated films of pure PMMA or undoped $NaGdF_4$−PMMA were lower than that of the reference one due to lower J_{sc}. In contrast, the solar cell coated with a DC-PMMA thin layer after one coating cycle generated better performance than the reference one based on the front bare FTO. The performance of DSSC with DC NCs was impacted by the $NaGdF_4:Eu^{3+}$ NC coating cycle number. Compared to the case of the reference cell, the PV performance improved with one and two coating cycles, then dropped when the number of the coating cycles increased. The best photovoltaic performance was achieved with one coating cycle. The best cell (Cell 3) shows a J_{sc} of 16.98 mA cm^{-2}, a V_{oc} of 0.765 V, a FF of 71.9%, and a η of 9.34%. The solar cell with $NaGdF_4:Eu^{3+}$ down-converters increased energy conversion efficiency by 10.3% relative to the device coated with the same thick undoped $NaGdF_4$−PMMA layer. The solar cell with $NaGdF_4:Eu^{3+}$ DC-PMMA layer prepared using two deposition cycle displays a J_{sc} of 16.42 mA cm^{-2}, a V_{oc} of 0.764 V, a FF of 71.9%, and a η of 9.02%. But, when the DC NC deposition cycle increased further, the DSSC showed poorer performance than the reference device. The best cell with $NaGdF_4:Eu^{3+}$ NCs demonstrated a 4.6% increase in short-circuit current density, a

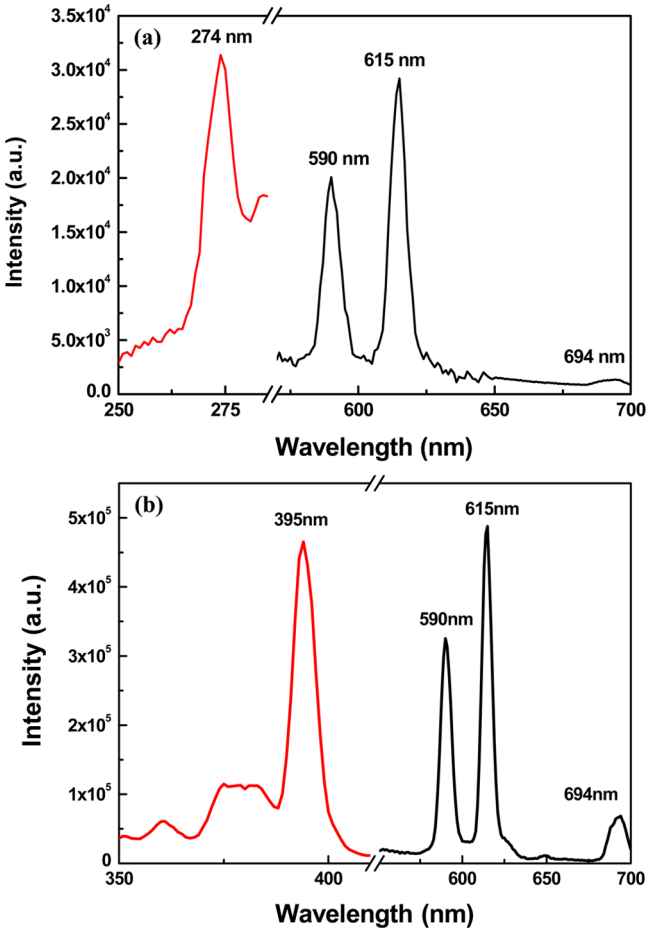

Figure 3. Room-temperature excitation and emission spectra of $NaGdF_4:Eu^{3+}$ NCs. (a) λ_{ex} = 274 nm, (b) λ_{ex} = 395 nm.

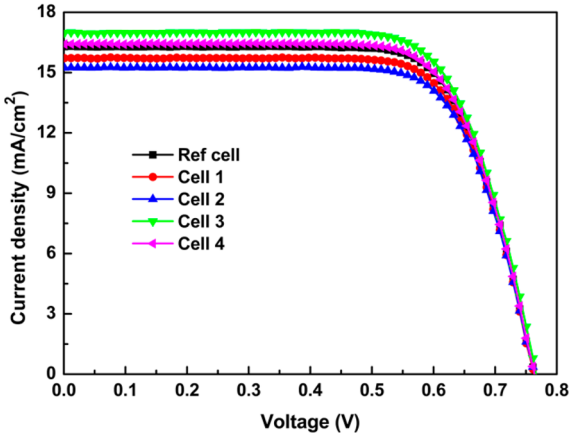

Figure 4. *J*–*V* characteristics of DSSCs based on the front bare FTO glass (ref cell), the FTO slides covered with pure PMMA (Cell 1), undoped $NaGdF_4$–PMMA (Cell 2) after one coating cycle, and $NaGdF_4:Eu^{3+}$–PMMA (Cell 3 and Cell 4) after one to two coating cycles.

ΔJ_{sc} = 0.74 mA cm^{-2} enhancement of the J_{sc}, and 4.5% raise in efficiency relative to the referenced one.

Figure 5 plots IPCE spectra of the reference cell with the front bare FTO slide and DSSCs with pure PMMA, undoped $NaGdF_4$, and $NaGdF_4:Eu^{3+}$ modified layers. From Figure 5, compared to the case of the uncoated device, only the introduction of the doped $NaGdF_4$–PMMA thin layer onto the front surface of a preformed DSSC can significantly enhance the IPCE of the device. With the addition of $NaGdF_4:Eu^{3+}$ NC by one coating cycle, the photon-to-carrier generation efficiency of the device (Cell 3) is conspicuously improved in the 250–600 nm region of the spectra. Specifically, similar to conventional DSSCs, the reference cell has no spectral response, and its IPCE values are near zero at λ < 300 nm due to the absorption of the FTO glass substrate. Nevertheless, at the wavelength of about 274 nm, the IPCE value reached 5–6% for cells with $NaGdF_4:Eu^{3+}$ DC-PMMA layers after one to two DC coating cycles. The IPCE spectra for both DSSCs with $NaGdF_4:Eu^{3+}$ DC NCs peaked at about 274 nm, which is ascribed to the $^8S_{7/2} \rightarrow {}^6I_J$ transitions of Gd^{3+} (Figure 3a). Gd^{3+} ions in $NaGdF_4:Eu^{3+}$ DC layers worked as a sensitizer to absorb the incident UV light and then transferred energy to the neighboring Eu^{3+} ions, resulting in the visible emission of Eu^{3+}. The emitted down-converted emission passed through the front FTO glass into the dye layer, where it excited electrons that then flowed into the titanium dioxide in the device, generating current and improving the spectral response and the IPCE in the ultraviolet portion of the solar spectrum. Moreover, the IPCE enhancement in 360–450 nm shown in Figure 5 can be associated with $^5D_0$–$^7F_1$, $^5D_0$–$^7F_2$, and $^5D_0$–$^7F_4$ transitions of Eu^{3+} under 395 nm excitation (Figure 3b). Therefore, the appearance of the IPCE peak at about 274 nm and IPCE enhancement in 360–450 nm clearly confirmed the DC luminescence effect from rare-earth Eu^{3+} ions in the down converting layer. The improvement in IPCE in these regions occurred because the incident light was absorbed by the DC nanophosphors before being absorbed by the PMMA or the FTO substrate, then reemitted as lower energy photons at longer wavelengths of 591 and 615 nm (Figure 3), where both PMMA or FTO glass substrate are transparent and the IPCE of the PV device is high. The presence of the $NaGdF_4:Eu^{3+}$ NCs provides a clear IPCE enhancement in the UV, as exhibited in

Table 1. Photovoltaic Performance Parameters for DSSCs Fabricated with Different Structured Photoanodes

sample	V_{oc} (V)	J_{sc}(mA/cm^2)	FF	η (%)
ref cell	0.765	16.24	0.720	8.94
cell 1	0.765	15.88	0.717	8.71
cell 2	0.764	15.23	0.728	8.47
cell 3	0.765	16.98	0.719	9.34
cell 4	0.764	16.42	0.719	9.02

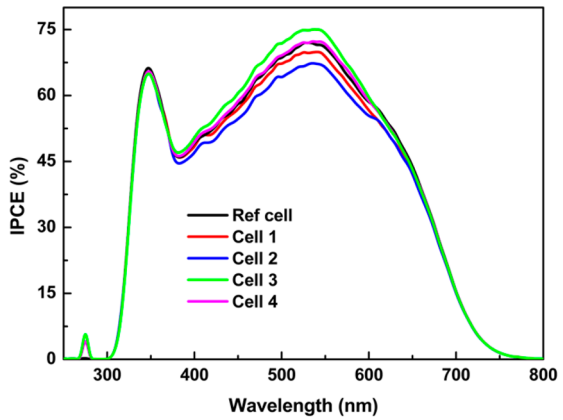

Figure 5. IPCE spectra of DSSCs fabricated with different structured photoanodes.

dx.doi.org/10.1021/am505086e | ACS Appl. Mater. Interfaces 2014, 6, 17454–17462

Figure 5, indicating that the increase of photocurrent in Cell 3 and Cell 4 can be attributed, to some extent, to the down conversion in the $NaGdF_4:Eu^{3+}$ nanophosphors for the UV light. Moreover, considering that the flux of solar radiation at about 274 nm is much lower than that in a wavelength range of 360−450 nm, the IPCE enhancement in the latter has more impact on the cell performance. From Figure 5, the improvement in IPCE for Cell 3 also obviously took place in the 450−600 nm region. In the visible and near-infrared (IR) region above 450 nm, because there is no PL signal from $NaGdF_4:Eu^{3+}$, luminescence DC cannot entirely explain the enhancement of IPCE shown in Figure 5. Figure 6 shows the

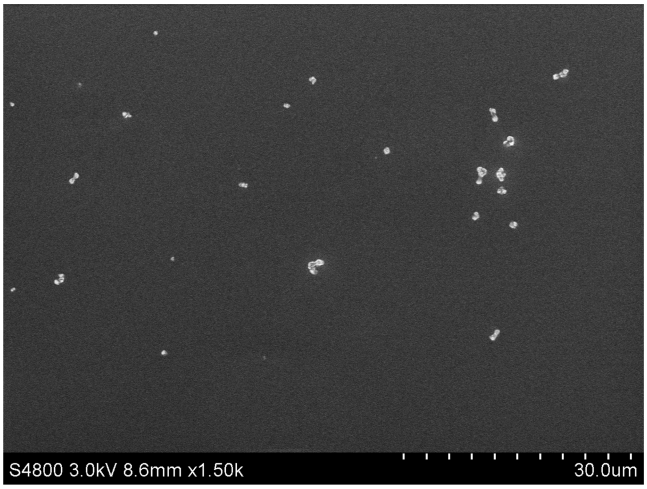

Figure 6. SEM image of $NaGdF_4:Eu^{3+}$−PMMA thin film on the front surface of a DSSC by one coating cycle.

typical SEM image of DC $NaGdF_4:Eu^{3+}$−PMMA thin film on the front surface of a DSSC at one deposition cycle. $NaGdF_4:Eu^{3+}$ NCs were very sparsely spread over the front surface of the device. The thickness of the DC-PMMA film is about 100 nm. As shown in Figure 6, $NaGdF_4:Eu^{3+}$ NCs were embedded within the PMMA on the flat surface of the cell, scattering of incident photons by the nanophosphors on the cell surface may couple normally incident light into the underlying photoanode, in which light can propagate laterally, rather than vertically, within the absorber. This may increase the light path length within the active region of the device to enable efficient generation of carriers. Therefore, the scattering by the $NaGdF_4:Eu^{3+}$ NCs could be essential for coupling and partially trapping light in the underlying photoanodes of the solar cells, which also led to the increase in quantum efficiency.[28,37]

It is worth mentioning that the concentration of $NaGdF_4:Eu^{3+}$ is very low in this work. We found that when the concentration of $NaGdF_4:Eu^{3+}$ NCs is very high during preparation of the DC-doped PMMA layers, the DC nanocrystals were difficult to disperse evenly in PMMA. Due to the strong scattering effects of aggregated DC crystals, more peaks appeared in the resultant IPCE spectra at $\lambda < 300$ nm, and the IPCE values were significantly higher for cells with high content $NaGdF_4:Eu^{3+}$ DC layers, reaching 20−60% at $\lambda < 300$ nm; this is similar to the results reported in ref 18. The latter demonstrated that the inclusion of luminescent down-shifting organic dye-doped PMMA resulted in the presence of random and multi external quantum efficiency (EQE) peaks and increased EQE values of encapsulated screen-printed crystalline silicon solar cells from near zero to 40% at $\lambda < 400$ nm. A ΔJ_{sc} of 0. 37 mA cm^{-2} was estimated from the measured EQE in the solar cell under the AM 1.5 spectrum, which is equivalent to a ∼1% increase in the relative efficiency of the module. Actually, J_{sc} can also be evaluated from IPCE spectra by integrating the AM 1.5 photon flux density and IPCE over the whole solar electromagnetic spectrum.[18] However, the J_{sc} values calculated directly from the IPCE shown in Figure 5 are smaller than those from the photovoltaic measurements in Table 1. There may be some causes for this result. Our $J-V$ and IPCE measurement systems are with 1 × 2 mm rectangular and 4 in. diameter round beam spots, respectively. $J-V$ and IPCE measurements were performed directly without masks in this work. Because the light spot of the IPCE system is much smaller than the DSSC cell (0.25 cm^2), IPCE measurements on the DSSCs without using a mask could be conducted with a relatively high accuracy, while the efficiency of the measured devices could be over assessed for up to 30% without using a suitable mask to do the $J-V$ measurements.[38,39] On the other hand, our IPCE measurement system is quite general. To measure IPCE, the DSSC under test and the reference detector were connected to a digital lock-in amplifier that isolated the signal from background noise. The IPCE equipment has no function to calculate J_{sc} from IPCE over its simulator spectrum. However, before measuring $J-V$ of the fabricated solar cells, the solar simulator was calibrated by a standard silicon solar cell. The light intensity was carefully checked and adjusted to 100 mW cm^{-2} on the surface of the measured cells to ensure relatively standard and accurate $J-V$ measurements. A distinct IPCE enhancement in an extra wide range from 250 to 600 nm was obtained by the DSSC with the DC layer after one deposition cycle. The J_{sc} value was significantly improved for the cell with this composite electrode.

The addition of a DC layer in a prefabricated photovoltaic device, however, can create additional interactions with light, inducing extra energy loss mechanisms in the solar cell.[16,28] In the previous study about the influence of down converting or shifting layers on unencapsulated solar cells, in most cases, the relevant efficiency increase was ascribed predominantly to a reduction in reflection of the front electrode rather than the DC luminescence effect from RE ions in down converting or shifting layers, and this was typically found in the case of cells with no antireflection coatings.[40−42] The reflection of the front electrode decreased due to a scattering effect of DC crystals or a gradual decrease of the refractive index from the front electrode substrate to the ambient air by adding the converting or shifting layer. The destructive interference of the scattered light from each interface of the down converting layer covered electrode may result in the reduction of reflection, causing the energy conversion efficiency gain in the solar cells. In our work, the deposited DC $NaGdF_4:Eu^{3+}$ NCs not only have efficient down conversion but also have high-quality transparency. The glass coated with pure DC NCs without PMMA is very close to the glass slide in transparency at 200−1100 nm wavelength range, as shown in Figure 7. Figure 8 shows the transmittance spectra of the bare FTO glass and the FTO slides covered with pure PMMA or undoped $NaGdF_4$−PMMA by one deposition cycle or $NaGdF_4:Eu^{3+}$−PMMA after one to three deposition cycles (referred to as DC-PMMA-1−3). PMMA, undoped $NaGdF_4$−PMMA, or doped $NaGdF_4$−PMMA was directly coated onto the glass surface of the FTO slides. The thickness of the coated layer after one deposition cycle is about 100 nm. The radiation was supposed to go through the coated layer,

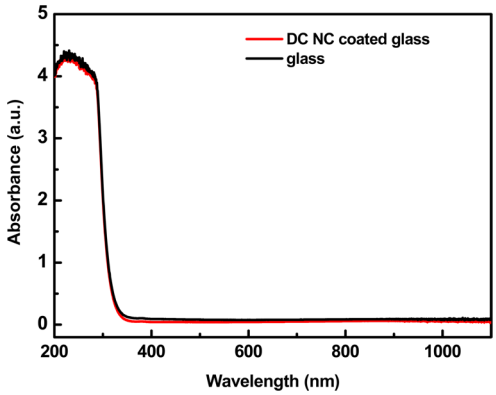

Figure 7. UV−vis spectra of the bare glass and $NaGdF_4:Eu^{3+}$ NC coated slides.

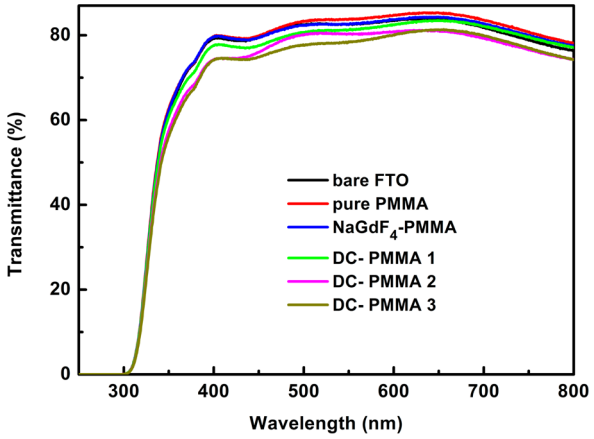

Figure 8. Transmittance spectra of the bare FTO glass and pure PMMA-, undoped $NaGdF_4$−PMMA-, and $NaGdF_4:Eu^{3+}$−PMMA-coated FTO slides.

glass, and FTO, as they do in the real device shown in Figure 1. As shown in Figure 8, the transmission properties of pure PMMA, $NaGdF_4$−PMMA, and DC-PMMA-1 are very similar to that of the bare FTO glass. Although undoped and doped $NaGdF_4$ NC modified FTO slides after one deposition cycle had similar optical transparency, the devices based on them achieved different performance, as shown in Figure 4 and Table 1. Compared to the case of the reference cell, the efficiency of Cell 2 decreased due to the addition of undoped $NaGdF_4$ NCs, whereas the efficiency of Cell 3 increased due to the addition of doped $NaGdF_4$ NCs. Therefore, the IPCE and power conversion efficiency gains in Cell 3 were mainly attributed to the effects of DC luminescence from rare-earth ions and scattering from nanophosphors in the down converting layer with 100 nm thickness, rather than to a reduction in reflection or an increase in transmission of the front electrode, as suggested in the previous work.[40−42] When the deposition cycle increased, the resulted DC modified FTO slides (DC-PMMA-2 and -3) showed lower and lower transmission due to the inclusion of more and more doped $NaGdF_4$ NCs and PMMA, further worsening its optical transparency, especially in the 500−600 nm region, where maximum IPCE is located, and degrading the performance of the related device.

In DSSCs with the $NaGdF_4:Eu^{3+}$ down converter, DC nanocrystals acted as both a scatterer and a DC spectral-splitter. Under the solar spectrum, the DC process altered the UV portion of the solar spectrum to better match the physical properties of the PV devices. The $NaGdF_4:Eu^{3+}$ NCs absorbed photons in the 270−400 nm range, and re-emitted light at a longer wavelength (575−620 nm) where the photovoltaic device has a considerably better response. Moreover, the scattering effect of DC NCs might play a positive role and result in IPCE enhancement in the 450−600 nm range for the cell with $NaGdF_4:Eu^{3+}$ NCs after one deposition cycle. Both the scattering and DC luminescence effects contributed to a gain in J_{sc} of 0.71 mA cm^2 and an increase of 4.5% in the efficiency of the DSSC. The total relative enhancement factor of efficiency up to 4.5% in our system is very close to the enhancement value calculated on an ideal system using semiconductor nanoparticles (NPs) as a DC layer and placing the down-converting material on top of a pre-existing solar cell.[28] Moreover, as we know, plasmonic nanostructures based on RE ions doped up conversion (UC) or DC NCs and noble metals such as Au or Ag NPs or nanofilms have been widely studied and applied for fluorescence signal amplification.[43−45] The UC nanocrystals act as luminescence up-shifting centers in the near-IR region, DC nanocrystals play the part of fluorescence down-shifting centers in the UV region, and the metal NPs or nanofilms help to enhance luminescence in the visible region. For example, we found that multilayered plasmonic structures of glass/Au/TiO_2/ $NaYF_4$:Yb, Er, Gd NCs achieved 150- and 192-fold enhancements for two green emissions (521 and 540 nm), respectively, at a 10 nm thick TiO_2 film under infrared 980 nm excitation.[45] Greatly enhanced DC luminescence from the $NaGdF_4$:Eu nanophosphors can be expected by employing a plasma-enhanced layer composed of Ag or Au NPs or nanofilms, and a dielectric (SiO_2, TiO_2, ZnO) spacer. $NaGdF_4$:Eu nanophosphors and a plasma-enhanced layer can be directly integrated into the DSSC surface for increasing the spectral response of the device, further enhancing fluorescence in the visible region to increase solar light absorption inside the active layer of DSSC, and therefore more significantly improving the photovoltaic performance of the DSSC.

4. CONCLUSIONS

$NaGdF_4:Eu^{3+}$ DC NCs were successfully synthesized via hydrothermal approach. The chemical composition and morphology of the as-prepared $NaGdF_4:Eu^{3+}$ NCs were characterized by XRD, SEM, and TEM measurements. DC layers consisting of poly(methyl methacrylate) (PMMA) doped with luminescent $NaGdF_4:Eu^{3+}$ were prepared and attached to the back (glass) of the TiO_2 anodes to make more efficient dye-sensitized solar cells. The influence of both doped and undoped $NaGdF_4$ NC layers on the photovoltaic device was compared and evaluated by the measurement of the device's IPCE. $NaGdF_4:Eu^{3+}$ nanocrystals acted as both a scatterer and a DC spectral-splitter in the device. The photovoltaic device added with of a 100 nm thick DC-PMMA layer demonstrated an obviously better spectral response in both ultraviolet and visible portions of the solar spectrum, contributing to an increase in J_{sc} of 0.74 mA cm^{-2} and a gain of 4.5% in the efficiency of the DSSC. It is expected that this approach will enable the potential utilization in other kinds of photovoltaic cells and the development of new technologies to exploit nanophosphors for energy devices.

AUTHOR INFORMATION

Corresponding Author

*E-mail: smhuang@phy.ecnu.edu.cn. Tel: 86 21 62233227. Fax: 86 21 62232053.

Notes

The authors declare no competing financial interest.

ACKNOWLEDGMENTS

This work was supported by the National Natural Science Foundation of China (Nos. 11274119 and 61275038) and the Large Instruments Open Foundation of East China Normal University.

REFERENCES

(1) O'Regan, B.; Grätzel, M. A Low-Cost, High-Efficiency Solar Cell Based on Dye-Sensitized Colloidal TiO_2 Films. *Nature* **1991**, *353*, 737−740.

(2) Chiba, Y.; Islam, A.; Watanabe, Y.; Komiya, R.; Koide, N.; Han, L. Dye-Sensitized Solar Cells with Conversion Efficiency of 11.1%. *Jpn. J. Appl. Phys., Part 2* **2006**, *45*, L638−L640.

(3) Mathew, S.; Yella, A.; Gao, P.; Humphry-Baker, R.; Curchod, B. F. E.; Ashari-Astani, N.; Tavernelli, I.; Rothlisberger, U.; Nazeeruddin, M. K.; Grätzel, M. Dye-Sensitized Solar Cells with 13% Efficiency Achieved Through the Molecular Engineering of Porphyrin Sensitizers. *Nat. Chem.* **2014**, *6*, 242−247.

(4) Grätzel, M. Photoelectrochemical Cells. *Nature* **2001**, *414*, 338−344.

(5) Grätzel, M. Dye-Sensitized Solar Cells. *J. Photochem. Photobiol., C* **2003**, *4*, 145−153.

(6) Grätzel, M. Solar Energy Conversion by Dye-Sensitized Photovoltaic Cells. *Inorg. Chem.* **2005**, *44*, 6841−6851.

(7) Jayaweera, P. V. V; Perera, A. G. U.; Tennakone, K. Why Grätzel's Cell Works so Well. *Inorg. Chim. Acta* **2008**, *361*, 707−711.

(8) Nazeeruddin, M. K.; Kay, A.; Rodicio, I.; Humphry-Baker, R.; Müller, E.; Liska, P.; Vlachopoulos, N.; Grätzel, M. Conversion of Light to Electricity by *cis*-X2Bis(2,2′-bipyridyl-4,4′-dicarboxylate)-ruthenium(II) Charge-Transfer Sensitizers (X = Cl-, Br-, I-, CN-, and SCN-) on Nanocrystalline Titanium Dioxide Electrodes. *J. Am. Chem. Soc.* **1993**, *115*, 6382−6390.

(9) Klein, C.; Nazeeruddin, M. K.; Liska, P.; Di Censo, D.; Hirata, N.; Palomares, E.; Durrant, J.; Grätzel, M. Synthesis of Novel Ruthenium Sensitizers and Their Application in Dye-Sensitized Solar Cells. *Inorg. Chem.* **2005**, *44*, 178−180.

(10) Lee, S.-H. A.; Abrams, N. M.; Hoertz, P. G.; Barber, G. D.; Halaoui, L. I.; Mallouk, T. E. Coupling of Titania Inverse Opals to Nanocrystalline Titania Layers in Dye-Sensitized Solar Cells. *J. Phys. Chem. B* **2008**, *112*, 14415−14421.

(11) Wegh, R. T.; Donker, H.; Oskam, K. D.; Meijerink, A. Visible Quantum Cutting in $LiGdF_4$:Eu^{3+} Through Downconversion. *Science* **1999**, *283*, 663−666.

(12) Wegh, R. T.; Van Loef, E. V. D.; Meijerink, A. Visible Quantum Cutting via Downconversion in $LiGdF_4$:Er^{3+},Tb^{3+} upon Er^{3+} $4f^{11} \rightarrow 4f^{10}5d$ Excitation. *J. Lumin.* **2000**, *90*, 111−122.

(13) Zhang, Q. Y.; Yang, G. F.; Jiang, Z. H. Cooperative Down Conversion in $GdAl_3(BO_3)_4$: RE^{3+}, Yb^{3+} (RE = Pr, Tb, and Tm). *Appl. Phys. Lett.* **2007**, *91*, 51903.

(14) van der Ende, B. M.; Aarts, L.; Meijerink, A. Lanthanide Ions as Spectral Converters for Solar Cells. *Phys. Chem. Chem. Phys.* **2009**, *11*, 11081−11095.

(15) Huang, X.; Han, S.; Huang, W.; Liu, X. Enhancing Solar Cell Efficiency: The Search for Luminescent Materials as Spectral Converters. *Chem. Soc. Rev.* **2013**, *42*, 173−201.

(16) Trupke, T.; Green, M.; Wurfel, P. Improving Solar Cell Efficiencies by Down-Conversion of High-Energy Photons. *J. Appl. Phys.* **2002**, *92*, 1668−1674.

(17) Klampaftis, E.; Ross, D.; McIntosh, K. R.; Richards, B. S. Enhancing The Performance of Solar Cells via Luminescent Down-Shifting of the Incident Spectrum: A Review. *Sol. Energy Mater. Sol. Cells* **2009**, *93*, 1182−1194.

(18) McIntosh, K. R.; Lau, G.; Cotsell, J. N.; Hanton, K.; Bätzner, D. L.; Bettiol, F.; Richards, B. S. Increase in External Quantum Efficiency of Encapsulated Silicon Solar Cells from a Luminescent Down-Shifting Layer. *Prog. Photovoltaics* **2009**, *17*, 191−197.

(19) Ptacek, P.; Schäfer, H.; Kömpe, K.; Haase, M. Crystal Phase Control of Luminescing α-$NaGdF_4$:Eu^{3+} and β-NaGdF4:Eu^{3+} Nanocrystals. *Adv. Funct. Mater.* **2007**, *17*, 3843−3848.

(20) Wang, F.; Fan, X.; Wang, M.; Zhang, Y. Multicolour PEI/$NaGdF_4$: Ce^{3+}, Ln^{3+} Nanocrystals by Single-Wavelength Excitation. *Nanotechnology* **2007**, *18*, 025701.

(21) Karbowiak, M.; Mech, A.; Bednarkiewicz, A.; Stręk, W.; Kępiński, L. Comparison of Different $NaGdF_4$:Eu^{3+} Synthesis Routes and Their Influence on Its Structural and Luminescent Properties. *J. Phys. Chem. Solids* **2005**, *66*, 1008−1019.

(22) Liu, J.; Yao, Q.; Li, Y. Effects of Downconversion Luminescent Film in Dye-Sensitized Solar Cells. *Appl. Phys. Lett.* **2006**, *88*, 173119.

(23) Lü, X.; Mou, X.; Wu, J.; Zhang, D.; Zhang, L.; Huang, F.; Xu, F.; Huang, S. Improved-Performance Dye-Sensitized Solar Cells Using Nb-Doped TiO_2 Electrodes: Efficient Electron Injection and Transfer. *Adv. Funct. Mater.* **2010**, *20*, 509−515.

(24) Hafez, H.; Saif, M.; Abdel-Mottaleb, M. Down-Converting Lanthanide Doped TiO_2 Photoelectrodes for Efficiency Enhancement of Dye-Sensitized Solar Cells. *J. Power Sources* **2011**, *196*, 5792−5796.

(25) Imahori, H.; Hayashi, S.; Umeyama, T.; Eu, S.; Oguro, A.; Kang, S.; Matano, Y.; Shishido, T.; Ngamsinlapasathian, S.; Yoshikawa, S. Comparison of Electrode Structures and Photovoltaic Properties of Porphyrin-Sensitized Solar Cells with TiO_2 and Nb, Ge, Zr-Added TiO_2 Composite Electrodes. *Langmuir* **2006**, *22*, 11405−11411.

(26) Saif, M.; Abdel-Mottaleb, M. Titanium Dioxide Nanomaterial Doped with Trivalent Lanthanide Ions of Tb, Eu, and Sm: Preparation, Characterization and Potential Applications. *Inorg. Chim. Acta* **2007**, *360*, 2863−2874.

(27) Feng, X.; Shankar, K.; Paulose, M.; Grimes, C. A. Tantalum-Doped Titanium Dioxide Nanowire Arrays for Dye-Sensitized Solar Cells with High Open-Circuit Voltage. *Angew. Chem.* **2009**, *121*, 8239−8242.

(28) Ze'ev, R. A.; Niv, A.; Zhang, X. Solar Energy Enhancement Using Down-Converting Particles: A Rigorous Approach. *J. Appl. Phys.* **2011**, *109*, 114905.

(29) Li, Z.; Li, X.; Liu, Q.; Chen, X.; Sun, Z.; Liu, C.; Ye, X.; Huang, S. M. Core/Shell Structured $NaYF_4$: Yb^{3+}/Er^{3+}/Gd^{3+} Nanorods With Au Nanoparticles or Shells for Flexible Amorphous Silicon Solar Cells. *Nanotechnology* **2012**, *23*, 025402.

(30) Wang, F.; Han, Y.; Lim, C. S.; Lu, Y.; Wang, J.; Xu, J.; Chen, H.; Zhang, C.; Hong, M.; Liu, X. Simultaneous Phase and Size Control of Upconversion Nanocrystals Through Lanthanide Doping. *Nature* **2010**, *463*, 1061−1065.

(31) Zhang, D.; Li, X.; Li, H.; Chen, S.; Sun, Z.; Yin, X.; Huang, S. Graphene-Based Counter Electrode for Dye-Sensitized Solar Cells. *Carbon* **2011**, *49*, 5382−5388.

(32) You, F.; Wang, Y.; Lin, J.; Tao, Y. Hydrothermal Synthesis and Luminescence Properties of $NaGdF_4$:Eu. *J. Alloys Compd.* **2002**, *343*, 151−155.

(33) Wang, S. B.; Li, Q.; Pei, L. Z.; Zhang, Q.-F. Zhang, Branch-Shaped $NaGdF_4$:Eu^{3+} Nanocrystals: Selective Synthesis, and Photoluminescence Properties. *Mater. Charact.* **2010**, *61*, 824−830.

(34) Li, C.; Quan, Z.; Yang, J.; Yang, P.; Lin, J. Highly Uniform and Monodisperse β-$NaYF_4$: Ln^{3+} (Ln = Eu, Tb, Yb/Er, and Yb/Tm) Hexagonal Microprism Crystals: Hydrothermal Synthesis and Luminescent Properties. *Inorg. Chem.* **2007**, *46*, 6329−6337.

(35) Liu, Y.; Tu, D.; Zhu, H.; Li, R.; Luo, W.; Chen, X. A Strategy to Achieve Efficient Dual-Mode Luminescence of Eu^{3+} in Lanthanides Doped Multifunctional $NaGdF_4$ Nanocrystals. *Adv. Mater.* **2010**, *22*, 3266−3271.

(36) Ghosh, P.; Tang, S.; Mudring, A.-V. Efficient Quantum Cutting in Hexagonal $NaGdF_4$:Eu^{3+} Nanorods. *J. Mater. Chem.* **2011**, *21*, 8640−8644.

(37) Derkacs, D.; Chen, W. V.; Matheu, P. M.; Lim, S. H.; Yu, P. K. L.; Yu, E. T. Nanoparticle-Induced Light Scattering for Improved Performance of Quantum-Well Solar Cells. *Appl. Phys. Lett.* **2008**, *93*, 091107.
(38) Ito, S.; Nazeeruddin, M. K.; Liska, P.; Comte, P.; Charvet, R.; Péchy, P.; Jirousek, M.; Kay, A.; Zakeeruddin, S. M.; Grätzel, M. Photovoltaic Characterization of Dye-Sensitized Solar Cells: Effect of Device Masking on Conversion Efficiency. *Prog. Photovoltaics* **2006**, *14*, 589−601.
(39) Li, X.; Zhang, D.; Yin, X.; Chen, S.; Shi, J.; Sun, Z.; Huang, S. The Effects of Polymer Gel Electrolyte Composition on Performance of Quasi-Solid-State Dye-Sensitized Solar Cells. *J. Solid State Electrochem.* **2011**, *15*, 1271−1277.
(40) Hovel, H.; Hodgson, R.; Woodall, J. The Effect of Fluorescent Wavelength Shifting on Solar Cell Spectral Response. *Sol. Energy Mater. Sol. Cells* **1979**, *2*, 19−29.
(41) Maruyama, T.; Shinyashiki, Y. Solar Cells Coated with Fluorescent Coloring Agent. *J. Electrochem. Soc.* **1998**, *145*, 2955−2957.
(42) Maruyama, T.; Shinyashiki, Y.; Osako, S. Energy Conversion Efficiency of Solar Cells Coated with Fluorescent Coloring Agent. *Sol. Energy Mater. Sol. Cells* **1998**, *56*, 1−6.
(43) Schietinger, S.; Aichele, T.; Wang, H.-Q.; Nann, T.; Benson, O. Plasmon-Enhanced Upconversion in Single NaYF4:Yb^{3+}/Er^{3+} Co-doped Nanocrystals. *Nano Lett.* **2010**, *10*, 134−138.
(44) Saboktakin, M.; Ye, X.; Oh, S. J.; Hong, S.-H.; Fafarman, A. T.; Chettiar, U. K.; Engheta, N.; Murray, C. B.; Kagan, C. R. Metal-Enhanced Upconversion Luminescence Tunable through Metal Nanoparticle−Nanophosphor Separation. *ACS Nano* **2012**, *6*, 8758−8766.
(45) Luo, Q.; Chen, Y.; Li, Z.; Zhu, F.; Chen, X.; Sun, Z.; Wei, Y.; Guo, H.; Zeng Bo Wang, Z. B.; Huang, S. Large Enhancements of $NaYF_4$:Yb/Er/Gd Nanorod Upconversion Emissions via Coupling with Localized Surface Plasmon of Au Film. *Nanotechnology* **2014**, *25*, 185401.